

Finding and breaking the realistic rate-distance limit of continuous variable quantum key distribution

Xuyang Wang,^{1,2,*} Siyou Guo,¹ and Pu Wang¹

¹State Key Laboratory of Quantum Optics and Quantum Optics Devices,
Institute of Opto-Electronics, Shanxi University, Taiyuan 030006, China

²Collaborative Innovation Center of Extreme Optics, Shanxi University, Taiyuan 030006, China
(Dated: May 27, 2022)

In this work, the rate-distance limit of continuous variable quantum key distribution is studied. We find that the excess noise generated on Bob's side and the method for calculating the excess noise restrict the rate-distance limit. Then, a realistic rate-distance limit is found. To break the realistic limit, a method for calculating the secret key rate using pure excess noise is proposed. The improvement in the rate-distance limit due to a higher reconciliation efficiency is analyzed. It is found that this improvement is dependent on the excess noise. From a finite-size analysis, the monotonicity of the Holevo bound versus the transmission efficiency is studied, and a tighter rate-distance limit is presented.

Introduction.—Quantum key distribution (QKD) allows two distant parties to share secret keys based on the laws of quantum physics. Anybody who eavesdrops on the information will be discovered, and the eavesdropped information can be subtracted to ensure security. It is expected that this technology will have great potential for applications in the future. Usually, QKD can be divided into discrete variable (DV) and continuous variable (CV) domains. The protocols in either domain have their advantages [1–3].

The first protocol in the CV domain was proposed in 1999 using squeezed states [4], and early CV protocols primarily focused on squeezed and entangled states [5–7]. In 2002, Grosshans and Grangier proposed the famous GG02 protocol [8]. This protocol enabled the realization of QKD by using only coherent states instead of nonclassical states. Then, the reverse reconciliation method was designed to beat the 3-dB limit. In 2003, the GG02 protocol was demonstrated experimentally [9]. Since then, CV QKD entered a period of rapid development. Various protocols were proposed and realized experimentally [10–20]. Prototypes were also realized, and some field tests were reported [21–23]. At present, CV QKD can be realized using low-cost off-the-shelf components and have good compatibility with classical communication systems [24]. Thus, it is considered a promising candidate for enabling the deployment of quantum cryptography in future networks. However, the longest distance of CV QKD remains limited to ~ 100 km in experiments. The reasons behind such a short distance are the reconciliation efficiency, excess noise, and finite-size effect. Usually, to minimize the finite-size effect, a typical method is increasing the total number of samples. Thus, improving the reconciliation efficiency, reducing the excess noise, and minimizing the finite-size effect are the main goals for developing methods that enhance the performance of various CV QKD systems.

Fortunately, owing to the incessant efforts of researchers worldwide, the reconciliation efficiency is con-

tinuously increased. At present, a reconciliation efficiency of 99%, which is close to the Shannon limit, can be achieved [25]. In this study, it was found that the improvement in the rate-distance limit due to higher reconciliation efficiency is dependent on the excess noise. Based on a detailed investigation of the CVQKD system, we found that the excess noise generated on Bob's side and the method for calculating the excess noise restrict the rate-distance limit. Then, a realistic rate-distance limit was found. To break the realistic limit, a method for calculating the secret key rate using pure excess noise is proposed. Revisiting the finite-size effect, we find a loophole due to the monotonicity of the Holevo bound. Then, a tighter rate-distance limit was used to ensure the security of system.

Rate-distance limits and experiment results of several typical protocols.—There are various protocols in CV QKD, such as one-way, two-way, and measurement-device-independent (MDI) protocols. Here, we mainly focus on one-way protocols that are experimentally demonstrated well. The rate-distance limits of several typical protocols are presented in Fig.1, and certain representative experimental results are also presented.

In Fig. 1, we can see that the transmission distances obtained by various experiments are less than or approximately 100 km, although the maximum transmission distance in theory can reach almost 500 km in the asymptotic case. To achieve reasonable rate-distance limits, the following parameters are used: reverse reconciliation efficiency $\beta = 0.95$, excess noise $\varepsilon = 0.01$, detection efficiency $\eta = 0.6$, electronic noise $v_e = 0.1$, and a transmission loss of 0.2 dB/km. The modulation variance is optimized according to the transmission distance (or transmission efficiency T). It is noted that all variances are normalized to the shot noise N_0 . For the entangled-state protocol, when the sender Alice uses homodyne detection, the same rate-distance limit as that for the squeezed-state protocol will be attained. When Alice uses heterodyne detection, the rate-distance limit

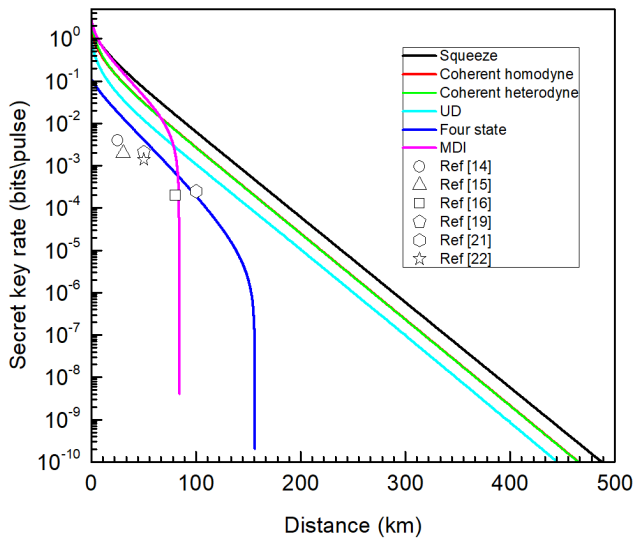


FIG. 1. Rate-distance limits and experimental results of several typical protocols.

will be that of the coherent-state protocol. Thus, the entangled-state protocol is not presented. For the presented protocols, the squeezed-state protocol with homodyne detection performs the best (black solid line). The coherent-state protocol with heterodyne detection (green solid line) performs better than that with homodyne detection (red solid line) at a short distance. With increasing distance, their rate-distance limits nearly converge to one line. Thus, the green solid line overlaps the red solid line. The Unidimensional (UD) coherent-state protocol has comparable performance with the normal two dimensional coherent protocols. It has the advantages of easy modulation and low costs and requires fewer random numbers [20, 26]. The non-Gaussian state protocols have the potential to realize high-speed gigahertz quantum communication using quaternary phase shift keying (QPSK) technology [27]. The modulated states are larger, and the performance is better. When the number of modulated states is eight, the performance approaches the two-dimensional coherent-state protocol [28]. Here, the typical four-state protocol is selected to be presented. The hot CV MDI protocol is also presented [29] because it becomes very sensitive to the detection efficiency, where the detection efficiency is set to $\eta = 1$ and the excess noise is set to $\varepsilon = 0.002$. To maximize the transmission distance, the middle part Clair is on Alice's side. A longest transmission distance of 80 km can be achieved.

Improvement in the rate-distance limit due to the reconciliation efficiency.—From a review of the experimental results, we can see that the realistic transmission distance is limited to ~ 100 km. One method for improving the performance is to improve the reconciliation efficiency. The reconciliation efficiency was recently improved to 0.99 [25]. This value is close to the Shannon

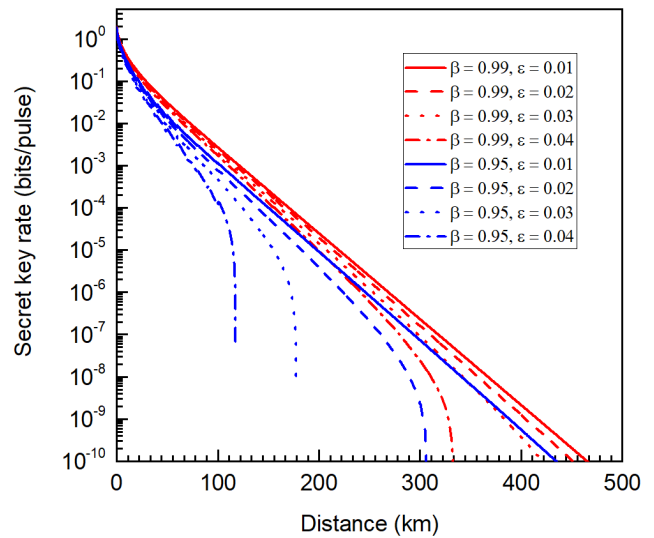


FIG. 2. Rate-distance limits for reconciliation efficiencies of $\beta = 0.95$ and $\beta = 0.99$.

limit. In the following, we will calculate the improvement in the rate-distance limit due to this higher efficiency based on coherent homodyne protocol (the famous GG02 protocol).

In Fig. 2, the red lines present the improved rate-distance limits due to a higher reconciliation efficiency of $\beta = 0.99$ at different excess noise conditions. Comparing them with the blue lines that represent the performance at a lower efficiency $\beta = 0.95$ with different excess noise, we observe that the improvement in the rate-distance limit is dependent on the excess noise. If the excess noise is larger, the improvement is more obvious. Because the limit of the distance at $\beta = 0.95$ and excess noise of 0.01 is far larger than the realistic transmission distance, we can infer that the reconciliation efficiency is not the primary reason limiting the rate-distance limits when the excess noise is ~ 0.01 .

Realistic Rate-distance limit.—Typically, there is a law that states that the excess noise is larger when the distance is higher. Considering that the excess noise ε_l from the fiber is small [30] and the excess noise ε_a generated on Alice's side is constant, this law remains applicable. In the experiment, controlling the excess noise to less than 0.01 at 100 km is extremely challenging [14, 19]. Through a careful analysis of the experimental system, we find that the excess noise ε_b generated on Bob's side and the method for calculating the excess noise result in this law. The excess noise generated on Bob's side is mainly attributed to the measurement error and the phase modulator used to switch the bases. To illustrate this law clearly, a typical model for describing the relation for the data in CV QKD is as follows:

$$y = t \cdot x + z, \quad (1)$$

where the variable y represents the quadrature received by Bob, and the variance of y is usually denoted as V_B . The variable x is the data used to modulate the state by Alice, and the variance of x is usually denoted as V_A . The variable z follows a Gaussian distribution with variance $\sigma^2 = N_0 + v_e + \eta T \varepsilon$ and a mean of zero. Thus, Eq. (1) can be transformed into a variance form as

$$V_B = \eta T (V_A + \varepsilon) + N_0 + v_e = \eta T V_A + \eta T \varepsilon + N_0 + v_e. \quad (2)$$

The ideal excess noise ε can be calculated by

$$\varepsilon = (V_B - \eta T V_A - N_0 - v_e) / \eta T = \varepsilon_a + \varepsilon_l + \varepsilon_b. \quad (3)$$

Typically, ε is normalized to the input port of the channel for security. We assume that the excess noise from Alice's setup, channel, and Bob's setup are stable. From Eq. (3), we can see that the noise will remain unchanged when the transmission efficiency varies. This contradicts the law that the excess noise is larger when the transmission distance is longer. We note the fact that ε_b generated on Bob's side is not attenuated with the channel transmission efficiency as shown in the following:

$$V_B = \eta T V_A + \eta T (\varepsilon_a + \varepsilon_l) + \varepsilon_b + N_0 + v_e. \quad (4)$$

The realistic excess noise ε_r , which reflects real experiment phenomena, can be calculated by

$$\varepsilon_r = (\eta T (\varepsilon_a + \varepsilon_l) + \varepsilon_b) / \eta T = \varepsilon_a + \varepsilon_l + \varepsilon_b / \eta T. \quad (5)$$

Although the excess noise terms ε_a , ε_l , ε_b are constant, the calculated realistic excess noise will increase when the transmission efficiency decreases. For example, a CV QKD system using the GG02 protocol has an excess noise of 0.01 when the total transmission efficiency ηT is 0.1 (39 km), $\varepsilon_a + \varepsilon_l = 0.005$, and $\varepsilon_b / \eta T = 0.005$. Then, the realistic excess noise (green dash-dot line) and the realistic rate-distance limits (blue solid line) are shown in Fig. 3.

In Fig. 3, although a high efficiency of $\beta = 0.99$ is used, because the realistic excess noise rapidly increases with the transmission distance, the maximum transmission distance is limited to about 100 km. The blue dashed line, blue dotted line, and blue dash-dot line are the conditions considering the finite-size effect which will be discussed in detail later. As Eve cannot access Bob's setup, if we can calibrate ε_b accurately and treat it similar to the electronic noise, the rate-distance limit in the asymptotic case will be represented by the black dashed line in Fig. 3 for pure excess noise, i.e., the condition $\varepsilon_p = \varepsilon_a + \varepsilon_l = 0.005$. The red solid line represents the secret key rate versus the distance with the ideal excess

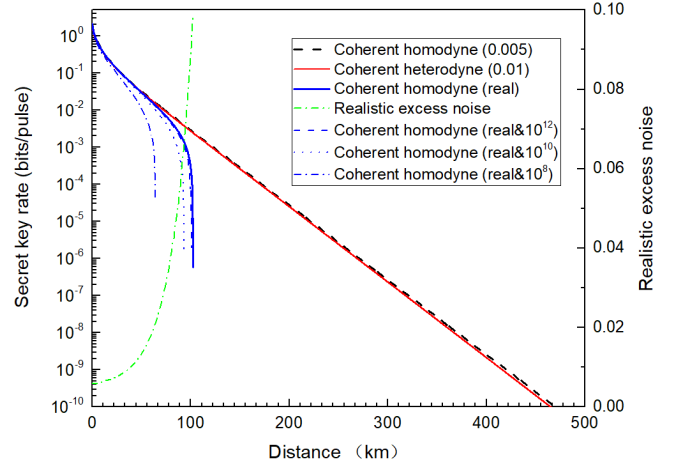


FIG. 3. Realistic rate-distance limits and the improved rate-distance limit.

noise of $\varepsilon = 0.01$. Thus, we can see that the measurement of ε_b is crucial for CV QKD to break the realistic rate-distance limit; meanwhile, we assume that it is also very challenging to achieve experimentally.

Rate-distance limit considering the finite-size effect.— In the above analysis, we mainly talk about the rate-distance limits in the asymptotic case. As the total number of data samples in experiments is finite, the finite-size effect must be considered. Thanks to the pioneering work of Leverrier [31], the finite-size effect has been explored and several important studies were subsequently performed [26, 32, 33]. Typically, the expression used to calculate the secret key rate considering the finite-size effect is

$$\Delta I_{AB}^f = (n/N) \cdot (\beta I_{AB} - S(y : E, \delta_{PE}) - \Delta(n, \delta)). \quad (6)$$

where n is number of data samples used to distill the secret key rate, m is number of the data samples used for parameter estimation, and $N = m + n$ represents the total number of samples. I_{AB} indicates the Shannon mutual information between Alice and Bob. $S(y : E, \delta_{PE})$ represents the maximum of the Holevo information compatible with the statistics, except with the probability δ_{PE} . $\Delta(n, \delta)$ is a correction term for the achievable mutual information in the finite case, and δ is the probability of an error during privacy amplification. Usually, conservative values of $\delta_{PE} = \delta = 10^{-10}$ are utilized.

The results of numerical calculations are presented in Fig. 4. The blue, black, and red solid curves represent the secret key rate ΔI_{AB} , Shannon mutual information I_{AB} , and the Holevo bound information $S(y : E)$ versus T respectively. The three solid curves are based on the condition that the pure excess noise $\varepsilon_p = 0.005$ has a constant value (green solid line). All dashed curves represent the corresponding information versus T under the

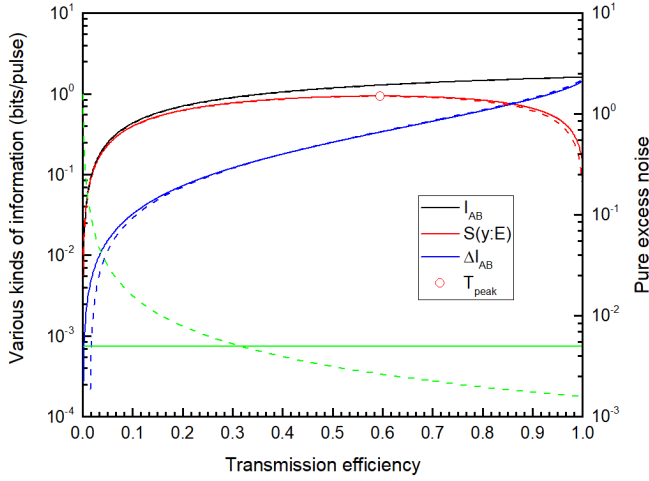


FIG. 4. Various kinds of information versus the transmission efficiency.

condition that the variable σ^2 is constant. The black dashed line overlaps the black solid line completely. In either case, the curve that represents $S(y : E)$ versus T is a convex curve. For a constant σ^2 , the pure excess noise (green dashed line) varies with the transmission efficiency, which is contradictory to real-life conditions. Thus, the condition that the pure excess noise is a constant value should be considered. The transmission efficiency that corresponds to the extreme point (red circle) of the red solid curve is denoted as T_{peak} , and its square root is t_{peak} . This means that calculating the maximum information $S(y : E, \delta_{PE})$ should be divided into two situations (different from [31]). When $t < t_{peak}$, the value t_{max} should be used to calculate $S(y : E, \delta_{PE})$. Here, t_{max} and the following t_{min} are the bounds of the confidence region of the estimated variable \hat{t} . At every point of this part red solid curve, the dependence of $S(y : E)$ on the variable t can be represented as

$$\left. \frac{\partial S(y : E)}{\partial t} \right|_{\sigma^2} > 0 \quad (7)$$

It is noted that at every point of red solid line, the constant pure excess noise corresponds to a constant σ^2 ; thus Eq. (7) can be established around a fixed transmission distance. When $t > t_{peak}$, t_{min} should be used to calculate $S(y : E, \delta_{PE})$. Thus, tighter rate-distance limits can be achieved, as shown in Fig. 5. From left to right, the total numbers of samples are 10^8 (blue lines), 10^{10} (green lines), and 10^{12} (red lines). The dashed curves are loose limits, and the solid curves are tight limits. When the total number of samples is larger, the difference between the solid and dashed lines of the same color is minimized. The black line represents the asymmetrical case. It is noted that the solid lines only reflect the expected case $E(\hat{t})$ or $E(\hat{\sigma})$. The estimated value, \hat{t} or $\hat{\sigma}^2$, may be any

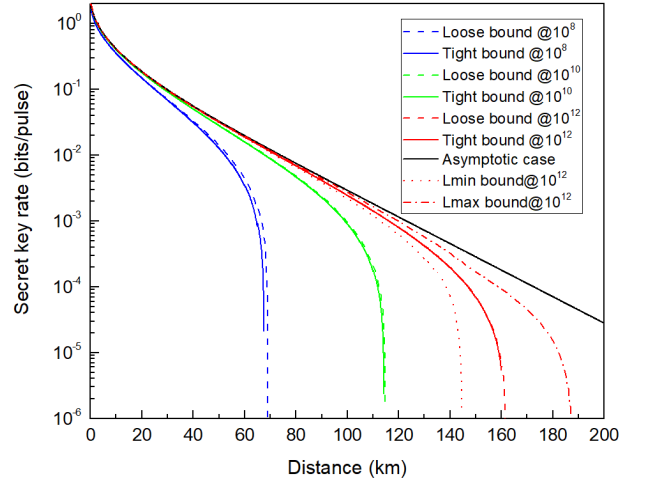


FIG. 5. Tight and loose rate-distance limits under pure excess noise conditions.

value in the confidence region $[t_{min}, t_{max}]$ or $[\sigma_{min}^2, \sigma_{max}^2]$ with a probability of $1 - \delta_{PE}$. Thus, the rate-distance limit should be distributed in a region among the red dotted line (L_{min} bound) and red dot-dash line (L_{max} bound) when the total number of samples is of the order of 10^{12} . The longest transmission distance is nearly 200 km. In an experiment, processing such a large number of data samples is very challenging and collecting these samples also requires the system to be very stable.

The realistic rate-distance limits considering the finite-size effect with different total numbers of samples are shown in Fig. 3. From left to right, the total numbers of samples for the blue dot-dash, blue dotted, and blue dashed lines are of the order of 10^8 , 10^{10} , and 10^{12} , respectively. These realistic rate-distance limits generally reflect the limitation of the CV QKD experimental system. The above analysis was mainly focused on the GG02 protocol; however, other protocols also have similar realistic rate-distance limits.

Conclusion.—In this paper, we study the realistic rate-distance limits of CV QKD. At first, we present the rate-distance limits and the experimental results of several typical protocols. Theoretical calculations indicate that the longest distance of 500 km can be achieved. However, the real transmission distance is limited to ~ 100 km. Based on the law that the excess noise increases with the transmission distance, we find that the excess noise generated on Bob's side and the method for calculating of the excess noise are the primary factors behind such a relationship. Thus, realistic rate-distance transmission limits are presented. The method for breaking the realistic rate-distance limits is to calibrate the excess noise on Bob's side and treat it as electronic noise. It is expected that this challenging experimental work could be performed in the future. We also found that the im-

provement in the rate-distance limit due to a higher reconciliation efficiency is dependent on the excess noise. If the excess noise is larger, the improvement is more obvious. Furthermore, the rate-distance limit considering the finite-size effect is restudied, and a tighter limit is presented.

Acknowledgments.—This research was supported by the Key Project of the Ministry of Science and Technology of China (2016YFA0301403), the National Natural Science Foundation of China (NSFC) (11504219 and 61378010), the Shanxi 1331KSC, and the Program for the Outstanding Innovative Teams of Higher Learning Institutions of Shanxi.

* wangxuyang@sxu.edu.cn

- [1] V. Scarani, H. Bechmann-Pasquinucci, N. J. Cerf, M. Dusek, N. Lutkenhaus, and M. Peev, *Rev. Mod. Phys.* 81, 1301 (2009).
- [2] C. Weedbrook, S. Pirandola, R. Garcia-Patron, N. J. Cerf, T. C. Ralph, J. H. Shapiro, and S. Lloyd, *Rev. Mod. Phys.* 84, 621 (2012).
- [3] S. Pirandola, R. Laurenza, C. Ottaviani, and L. Banchi, *Nat. Commun.* 8, 15043 (2017).
- [4] T. C. Ralph, *Phys. Rev. A* 61, 010303 (1999).
- [5] N. J. Cerf and M. Levy, and G. VanAssche, *Phys. Rev. A* 63, 052311 (2001).
- [6] D. Gottesman and J. Preskill, *Phys. Rev. A* 63, 022309 (2001).
- [7] C. Silberhorn, N. Korolkova, and G. Leuchs, *Phys. Rev. Lett.* 88, 167902 (2002).
- [8] F. Grosshans and P. Grangier, *Phys. Rev. Lett.* 88, 057902 (2002).
- [9] F. Grosshans, G. Van Assche, J. Wenger, R. Brouri, N. J. Cerf, and P. Grangier, *Nature* 421, 238, (2003).
- [10] C. Weedbrook, A. M. Lance, W. P. Bowen, T. Symul, T. C. Ralph, and P. K. Lam, *Phys. Rev. Lett.* 93, 170504 (2004).
- [11] R. Garcia-Patron and N. J. Cerf, *Phys. Rev. Lett.* 97, 190503 (2006).
- [12] J. Lodewyck, M. Bloch, R. Garcia-Patron, S. Fossier, E. Karpov, E. Diamanti, T. Debuisschert, N. J. Cerf, R. Tualle-Brouri, S. W. McLaughlin, and P. Grangier, *Phys. Rev. A* 76, 042305 (2007).
- [13] X. Y. Wang, Z. L. Bai, S. F. Wang, Y. M. Li, and K. C. Peng, *Chin. Phys. Lett.* 30, 010305 (2013).
- [14] P. Jouguet, S. Kunz-Jacques, A. Leverrier, P. Grangier, and E. Diamanti, *Nat. Photon.* 7, 378 (2013).
- [15] X. L. Su, *Chin. Sci. Bull.* 59, 1083 (2013).
- [16] V. C. Usenko and F. Grosshans, *Phys. Rev. A* 92, 062337 (2015).
- [17] C. Wang, D. Huang, P. Huang, D. Lin, J. Peng, and G. Zeng, *Sci. Rep.* 5, 14607 (2015).
- [18] B. Qi, P. Lougovski, R. Pooser, W. Grice, and M. Bobrek, *Phys. Rev. X* 5, 041009 (2015).
- [19] D. Huang, P. Huang, D. Lin, and G. Zeng, *Sci. Rep.* 6, 19201 (2016).
- [20] X. Y. Wang, W. Y. Liu, P. Wang, and Y. M. Li, *Phys. Rev. A* 95, 062330 (2017).
- [21] S. Fossier, E. Diamanti, T. Debuisschert, A. Villing, R. Tualle-Brouri, and P. Grangier, *New J. Phys.* 11, 045023 (2009).
- [22] D. Huang, P. Huang, H. Li, T. Wang, Y. Zhou, and G. Zeng, *Opt. Lett.* 41, 3511 (2016).
- [23] Y. M. Li, X. Y. Wang, Z. L. Bai, W. Y. Liu, S. S. Yang, and K. C. Peng, *Chin. Phys. B* 26, 040303 (2017).
- [24] F. Karinou, H. H. Brunner, C. F. Fung, L. C. Comandar, S. Bettelli, D. Hillerkuss, M. Kuschnerov, S. Mikroulis, D. Wang, C. Xie, M. Peev, and A. Poppe, *IEEE Photonic Tech. Lett.* 30, 650 (2018).
- [25] M. Milicevic, C. Feng, L. M. Zhang and P. G. Gulak, *NPJ Quantum Inf.* 4, 21 (2018).
- [26] P. Wang, X.Y. Wang, J.Q. Li, and Y.M. Li, *Opt. Express* 25, 27995 (2017).
- [27] Z. Qu, I. B. Djordjevic, and M. A. Neifeld. 41, 5507 (2016).
- [28] A. Leverrier and P. Grangier, *Phys. Rev. A* 83, 042312 (2011).
- [29] S. Pirandola, C. Ottaviani, G. Spedalieri, C. Weedbrook, S. L. Braunstein, S. Lloyd, T. Gehring, C. S. Jacobsen, and U. L. Andersen, *Nat. Photonics* 9, 397 (2015).
- [30] J. Lodewyck, T. Debuisschert, R. Tualle-Brouri, and P. Grangier, *Phys. Rev. A* 72, 050303(R) (2005).
- [31] A. Leverrier, F. Grosshans, and P. Grangier, *Phys. Rev. A* 81, 062343 (2010).
- [32] P. Papanastasiou, C. Ottaviani, and S. Pirandola, *Phys. Rev. A* 96, 042332 (2017).
- [33] X. Zhang, Y. Zhang, Y. Zhao, X. Wang, S. Yu, and H. Guo, *Phys. Rev. A* 96, 042334 (2017).